ORIGINAL ARTICLE

Carboxylesterase 1 family knockout alters drug disposition and lipid metabolism

Changpei Gan[a], Jing Wang[a], Alejandra Martínez-Chávez[a,b],
Michel Hillebrand[b], Niels de Vries[b], Joke Beukers[b], Els Wagenaar[a],
Yaogeng Wang[a], Maria C. Lebre[a], Hilde Rosing[b],
Sjoerd Klarenbeek[d], Rahmen Bin Ali[e], Colin Pritchard[e],
Ivo Huijbers[e,#], Jos H. Beijnen[a,b,c], Alfred H. Schinkel[a,*]

[a]*Division of Pharmacology, the Netherlands Cancer Institute, Amsterdam 1066 CX, the Netherlands*
[b]*Department of Pharmacy & Pharmacology, the Netherlands Cancer Institute, Amsterdam 1066 CX, the Netherlands*
[c]*Division of Pharmacoepidemiology and Clinical Pharmacology, Utrecht Institute for Pharmaceutical Sciences, Utrecht University, Utrecht 3584 CS, the Netherlands*
[d]*Experimental Animal Pathology Facility, the Netherlands Cancer Institute, Amsterdam 1066 CX, the Netherlands*
[e]*Mouse Clinic for Cancer and Aging (MCCA) Transgenic Facility, the Netherlands Cancer Institute, Amsterdam 1066 CX, the Netherlands*

Abstract The mammalian carboxylesterase 1 (Ces1/CES1) family comprises several enzymes that hydrolyze many xenobiotic chemicals and endogenous lipids. To investigate the pharmacological and physiological roles of Ces1/CES1, we generated *Ces1* cluster knockout (*Ces1$^{-/-}$*) mice, and a hepatic human CES1 transgenic model in the *Ces1$^{-/-}$* background (TgCES1). *Ces1$^{-/-}$* mice displayed profoundly decreased conversion of the anticancer prodrug irinotecan to SN-38 in plasma and tissues. TgCES1 mice exhibited enhanced metabolism of irinotecan to SN-38 in liver and kidney. Ces1 and hCES1 activity increased irinotecan toxicity, likely by enhancing the formation of pharmacodynamically active SN-38. *Ces1$^{-/-}$* mice also showed markedly increased capecitabine plasma exposure, which was moderately decreased in TgCES1 mice. *Ces1$^{-/-}$* mice were overweight with increased adipose tissue, white adipose tissue inflammation (in males), a higher lipid load in brown adipose tissue, and impaired blood glucose tolerance (in males). These phenotypes were mostly reversed in TgCES1 mice. TgCES1 mice displayed

increased triglyceride secretion from liver to plasma, together with higher triglyceride levels in the male liver. These results indicate that the carboxylesterase 1 family plays essential roles in drug and lipid metabolism and detoxification. $Ces1^{-/-}$ and TgCES1 mice will provide excellent tools for further study of the *in vivo* functions of Ces1/CES1 enzymes.

1. Introduction

Mammalian carboxylesterases (rodents: Ces, human: CES) belong to the superfamily of serine hydrolases. They can cleave carboxylic acid ester, amide, and thioester bonds in substrates[1−4]. There are five Ces/CES families based on amino acid sequence identity. Six human *CES* genes have been identified, and twenty mouse *Ces* genes[5]. Ces/CES enzymes can participate in detoxifying various drugs and environmental toxicants, and in metabolic activation of some prodrugs[6]. Some also hydrolyze endogenous lipids such as triglycerides, cholesteryl esters and retinyl esters[7]. Several Ces/CES enzymes are not only expressed in pharmacokinetically relevant tissues (liver, small intestine and kidney), but also in lipid-storing and -metabolizing locations (white and brown adipose tissues)[8]. They are therefore thought to play important roles in both drug metabolism and lipid homeostasis.

Among the five Ces/CES families, most attention has been paid to Ces1/CES1 and Ces2/CES2[9,10]. In humans, the CES1 enzyme is abundantly expressed in liver parenchyma cells, primarily in the endoplasmic reticulum (ER), and to a lower extent in adipose tissue, kidney, and macrophages[8]. Interestingly, *CES1* mRNA levels in adipose tissue positively correlate with adiposity in several independent studies[11−13]. CES1 has broad substrate specificity, encompassing narcotics (heroin, cocaine), drugs (irinotecan, capecitabine, oseltamivir and methylphenidate) and endogenous lipids (triglycerides, cholesteryl esters)[7,14]. Several single nucleotide polymorphisms have been identified in the *CES1* gene, which are directly associated with altered pharmacokinetics of several drugs[14]. Eight mouse *Ces1* genes (*Ces1a* to *Ces1h*) are located in tandem on chromosome 8[5]. Ces1 enzymes have a fairly wide and unique tissue distribution, for example, seven Ces1 enzymes (Ces1a to Ces1g) are expressed in the liver to different degrees; a special case is Ces1c which is primarily secreted from liver into plasma due to lack of an ER retention signal, presenting an important species difference with human CES1, which is not secreted; Ces1d is most highly expressed in adipose tissue, and Ces1f in kidney[8]. For the mouse Ces1 enzymes, several endogenous substrates, especially lipids, have been recognized in *in vitro* assays. Ces1d and Ces1f exhibit triglyceride hydrolase activity[15,16]; retinyl ester can be hydrolyzed by Ces1e[17].

Valuable insights particularly into physiological roles of Ces1/CES1 enzymes have been gained from genetically modified mouse models. It has been demonstrated that hepatic human CES1 is involved in VLDL (very low density lipoprotein) assembly and secretion in inducible transgenic mice[18]. Moreover, hepatic CES1 may also participate in cholesterol handling and can even influence atherosclerosis development[19]. Several single *Ces1* knockout mouse models (*Ces1c*, *Ces1d* and *Ces1g*) have been generated for drug and lipid metabolism studies[20−22]. Even though these Ces1 enzymes share high amino acid sequence identity with each other[5,7], the *Ces1* knockout mouse models exhibit distinct and sometimes even opposite phenotypes: lower blood lipids and improved glucose tolerance were observed in *Ces1d* knockout mice[21], whereas loss of *Ces1g* led to obesity, hepatic steatosis, and hyperlipidemia[22].

To our knowledge, there are as yet no individual *Ces1a*, *Ces1b*, *Ces1e*, *Ces1f* or *Ces1h in vivo* mouse models, limiting the possibilities to thoroughly understand the functions of mouse Ces1 enzymes *in vivo*. Furthermore, current human CES1 transgenic mice were generally generated and studied in a wild-type (WT) *Ces1*-proficient background, making it possibly challenging to translate these results to humans. In this study we aimed to systematically investigate the *in vivo* influence of Ces1/CES1 enzymes on drug and lipid metabolism by generating and analyzing *Ces1* cluster knockout mice and hepatic human CES1 transgenic mice in a mouse *Ces1* cluster knockout background.

2. Materials and methods

2.1. Animals

Mice were housed in an environment-controlled room with a 12-h light/12-h dark cycle. They were fed a medium-fat diet from Special Diets Services (TransBreed (E) 801,228, fat content 10% by weight, 24% by calories, Essex, UK) and acidified water *ad libitum*. All were of a comparable genetic background (FVB/NRj) and between 9 and 16 weeks of age. All mice were fertile and produced at the expected Mendelian frequencies.

2.2. Generation of $Ces1^{-/-}$ and TgCES1 mice

Details of developing $Ces1^{-/-}$ and TgCES1 mice are described in supporting methods (Supporting Information). To dilute potential off-target effects caused by CRISPR/Cas9 targeting, the *Ces1* deletion allele was backcrossed with wild-type FVB/NRj mice for three generations before breeding to homozygosity.

2.3. Plasma and tissue pharmacokinetic experiments

Irinotecan and SN-38 used for the quantification reference standards were from Sigma−Aldrich (Saint Louis, MO, USA, purity ≥ 97%). Chemotherapy-grade irinotecan hydrochloride trihydrate (20 mg/mL, corresponding to 17.33 mg/mL irinotecan, obtained from Fresenius Kabi, Cheshire, UK) was diluted with saline to 5 mg/mL for *in vivo* mouse experiments. For both the oral and i.v. experiments, 4 μL of drug solution per gram of body weight was administered to male mice (*n* = 3−7). Blood samples were collected from the tail vein at various time points using heparinized capillary tubes (Sarstedt, Germany). At 8 h (oral) or 4 h (i.v.), the mice were sacrificed under isoflurane anesthesia,

and heparin-blood sampling by cardiac puncture followed by cervical dislocation. Several tissues were collected and rapidly frozen at −30 °C. Prior to analysis, organs were homogenized on ice in 4% (w/v) BSA (Roche Diagnostics, Mannheim, Germany) in water and stored at −30 °C until analysis. Blood samples were centrifuged at 2700 × g for 6 min at 4 °C after collection, and the plasma fraction was collected and stored at −30 °C until analysis. Levels of irinotecan and SN-38 were analyzed by HPLC-fluorescence as described previously. The lower limit of quantification for irinotecan was 7.5 ng/mL, and for SN-38 5 ng/mL[23].

The capecitabine (Carbosynth, Berkshire, UK) working solution was 50 mg/mL, including 3% (v/v) DMSO, 4% Tween 80/ ethanol (1:1; v/v) and 40 mmol/L NaAc (pH 4.2). It was orally administered by gavage to female mice (n = 4−7) at a dose of 500 mg/kg, using a volume of 10 μL/g body weight. The experimental procedure was the same as described above for the irinotecan oral study. HPLC−MS/MS was used to measure levels of capecitabine and its 4 metabolites as described previously[24].

2.4. Analysis of triglyceride secretion in vivo

Mice were fasted for 16 h and then injected intraperitoneally with 1 g/kg of Poloxamer-407 (Sigma−Aldrich, Steinheim, Germany) in 0.9% NaCl. Blood samples were collected from the tail vein before injection and 1, 2, 3, and 4 h after injection of the lipase inhibitor. Plasma was prepared and triglyceride levels were analyzed by LabAssay Triglyceride Kit (Wako Chemicals, Osaka, Japan).

2.5. Measurement of plasma and hepatic triglyceride and plasma glycerol and free fatty acids

The triglyceride level in plasma was measured using a Roche Cobas analyzer. Hepatic lipid was first isolated by Lipid Extraction Kit (PK-CA577-K216, PromoCell, Heidelberg, Germany), and the hepatic triglyceride level was determined by LabAssay Triglyceride Kit (Wako Chemicals, Osaka, Japan). Commercially available kits were used to measure plasma glycerol and free fatty acid levels (Products No. 2913 and 3055, Instruchemie, The Netherlands).

2.6. Glucose and insulin tolerance tests

For the glucose tolerance test, mice fasted for 16 h received orally administered glucose monohydrate (Merck, Darmstadt, Germany, 1 g/kg body weight). Blood glucose levels in tail vein samples were monitored before (0 min) and after glucose infusion at various time points (15, 30, 60, 90, and 120 min) with an ACCU-CHEK Performa glucose meter (Roche Diagnostics, Mannheim, Germany). For the insulin tolerance test, mice fasted for 6 h were intraperitoneally injected with insulin (Sigma−Aldrich, Steinheim, Germany, 0.5 U/kg body weight), followed by measurement of blood glucose as described above.

2.7. Real-time PCR analysis

RNA from mouse liver and small intestine was isolated by RNeasy Mini Kit, RNA from mouse brown adipose tissue was isolated by RNeasy Lipid Tissue Mini Kit (QIAGEN GmbH, Hilden, Germany). Subsequent cDNA synthesis was carried out using Maxima First Strand cDNA Synthesis Kit (Thermo Scientific, Vilnius, Lithuania), and real-time PCR using specific primers (QIAGEN GmbH, Hilden, Germany) for mouse Ces1, Ces2, Ces3 genes, thermogenic genes, hepatic fatty acid and triglyceride synthesis genes were performed as described previously[25,26].

2.8. Western blot analysis

Crude membrane fractions were isolated from mouse liver, kidney, and small intestine as described previously[26]. The microsomal protein was quantified by the BCA protein Assay Kit (Thermo Scientific, Rockford, USA). After transfer, blots were probed with rabbit anti-human CES1 monoclonal antibody (ab53008, Abcam) (dilution 1:20,000), and rabbit anti-β-Actin monoclonal antibody (#4970, Cell Signaling) (dilution 1:2000), followed by HRP-labeled goat anti-rabbit antibody (Dako Denmark A/S, Glostrup, Denmark).

2.9. Histological and immunohistochemical analysis

Isolated tissues were handled as described previously. Hematoxylin and eosin (H&E)-stained, and Oil Red O-stained sections were analyzed for pathological changes as previously described[26]. Immunohistochemistry on wild-type, Ces1−/− and TgCES1 tissues was conducted with a rabbit anti-human CES1 monoclonal antibody (ab53008, Abcam), and secondary antibody conjugated to HRP-labeled polymers (EnVision + System-HRP; DakoCytomation, Glostrup, Denmark).

2.10. Pharmacokinetic calculations and statistics

Mean concentrations (ng/mL) for each time point were used to calculate the area under the plasma concentration versus time curve (AUC) from time 0 to the last sampling point by the linear trapezoidal rule. Two-tailed unpaired Student's t test was used to assess the significance of differences between two sets of data. One-way ANOVA followed by Tukey's post hoc test was used to determine the significance of differences among three groups. Data are presented as mean ± standard deviation (SD); differences were considered to be statistically significant when P was less than 0.05.

2.11. Study approval

All mouse experiments were approved by the Institutional Animal Care and Use Committee (Animal Experiments Review Board) of the Netherlands Cancer Institute, complying with Dutch and E.U. legislation.

3. Results

3.1. Generation of Ces1 cluster knockout mice

The mouse Ces1 gene cluster (∼360 kb) on chromosome 8 harbors 8 individual Ces1 genes (Fig. 1A). We initially aimed to obtain conditional Ces1 cluster knockout (Ces1−/−) mice by inserting loxP sites flanking the Ces1 cluster using CRISPR/Cas9 methodology[27], followed by Cre-mediated deletion (Fig. 1B). Coinjection of Cas9 mRNA, two gRNAs and two single-stranded homologous recombination DNA oligos into FVB/NRj zygotes successfully generated conditional mutant alleles in offspring mice, with insertion of loxP sites flanking the mouse Ces1 cluster. However, we also found several mouse lines among the offspring with a direct and full deletion of the Ces1a−Ces1h locus. DNA sequencing revealed that
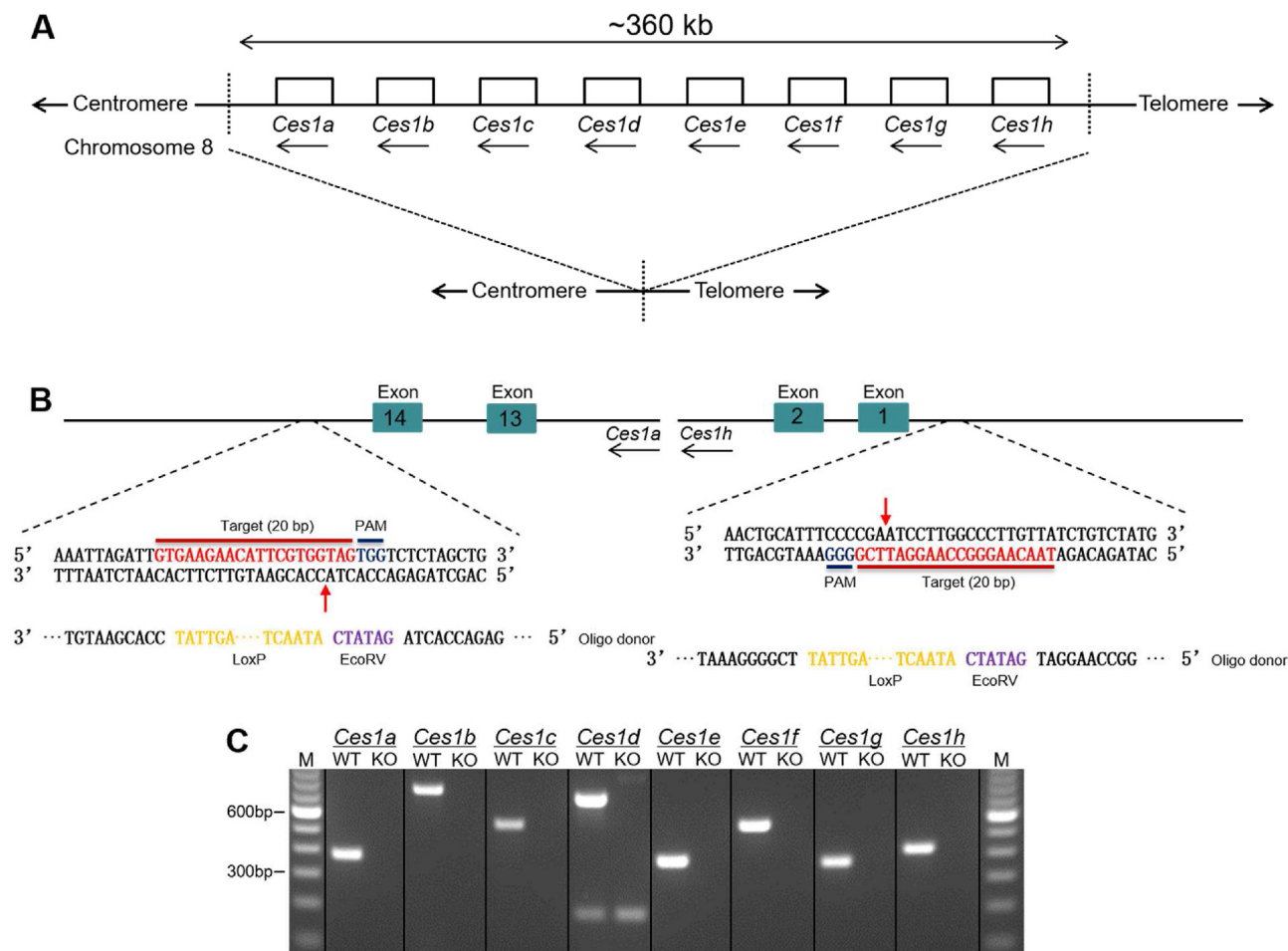
Figure 1 Generation of Ces1$^{-/-}$ mice. (A) Schematic overview of the strategy for deletion of the *Ces1* cluster genes. The cutting sites (stippled lines) were targeted just upstream and downstream of the *Ces1* cluster by CRISPR/Cas9 methodology. Subsequently the whole *Ces1* cluster was deleted, yielding a product allele as depicted below the *Ces1* locus (stippled line). Gene sizes and intergenic distances are not to scale. Each white box represents a single gene. (B) Detail of the Cas9/sgRNA/oligo targeting sites downstream and upstream of the *Ces1* cluster. The sgRNA coding sequence is underlined and labeled in red. The PAM sequence is shown in blue. The Cas9 cutting sites are indicated by red arrows. In the oligo donor sequence, the *loxP* site is indicated in yellow, and the restriction site sequence in purple. The donor oligos contain 60 bp homologies on both sides flanking the planned double-strand breaks. (C) PCR analysis of all *Ces1* genes in tail DNA of wild-type (WT) and *Ces1*$^{-/-}$ mice; KO: *Ces1* cluster knockout.

these lines were generated by direct ligation of the targeted Cas9 cutting sites flanking *Ces1a* and *Ces1h*, often with some additional nucleotide insertions and deletions, but also one line that was a clean hybrid of the planned Cas9 cutting sites (Supporting Information Fig. S1). As two independent *Ces1* cluster deletion alleles could be readily bred to homozygosity, and the resulting two independent *Ces1*$^{-/-}$ founder lines were normally viable and fertile, we mothballed the *Cre-loxP* approach and focused on analysis of the direct deletion strains.

The PCR products for all *Ces1* genes present in WT were absent in *Ces1*$^{-/-}$ mice (Fig. 1C). Accordingly, RT-PCR analysis demonstrated a sharp "downregulation" of RNAs for all significantly expressed *Ces1* genes in liver and small intestine of *Ces1*$^{-/-}$ compared with WT male mice (Supporting Information Table S2). We also checked the expression levels of the functionally and structurally related *Ces2* and *Ces3* gene families. No significant or meaningful changes were detected between WT and *Ces1*$^{-/-}$ male mice (Table S2).

3.2. Loss of all Ces1 enzymes decreases the formation of SN-38 from irinotecan

The anticancer prodrug irinotecan is approved for the treatment of metastatic colorectal cancer and small cell lung cancer[25]. It is converted by esterases into the active metabolite, SN-38 (Supporting Information Scheme S1). We administered irinotecan hydrochloride trihydrate (20 mg/kg) orally or i.v. to male WT and *Ces1*$^{-/-}$ mice. Levels of irinotecan and SN-38 in plasma were analyzed by HPLC-fluorescence[23]. Plasma AUCs of irinotecan were 17.2- and 1.9-fold higher in *Ces1*$^{-/-}$ *versus* WT mice after oral and i.v. dosing, respectively (Fig. 2A, C and Supporting Information Table S3). In WT mice, the plasma concentration of irinotecan at all time points after oral administration was below the limit of detection (12.5 ng/mL) (Fig. 2A), suggesting extensive hydrolysis of oral irinotecan in WT mice. Loss of Ces1 enzymes resulted in markedly decreased hydrolysis of irinotecan in *Ces1*$^{-/-}$ mice, and hence increased irinotecan plasma levels. However, after
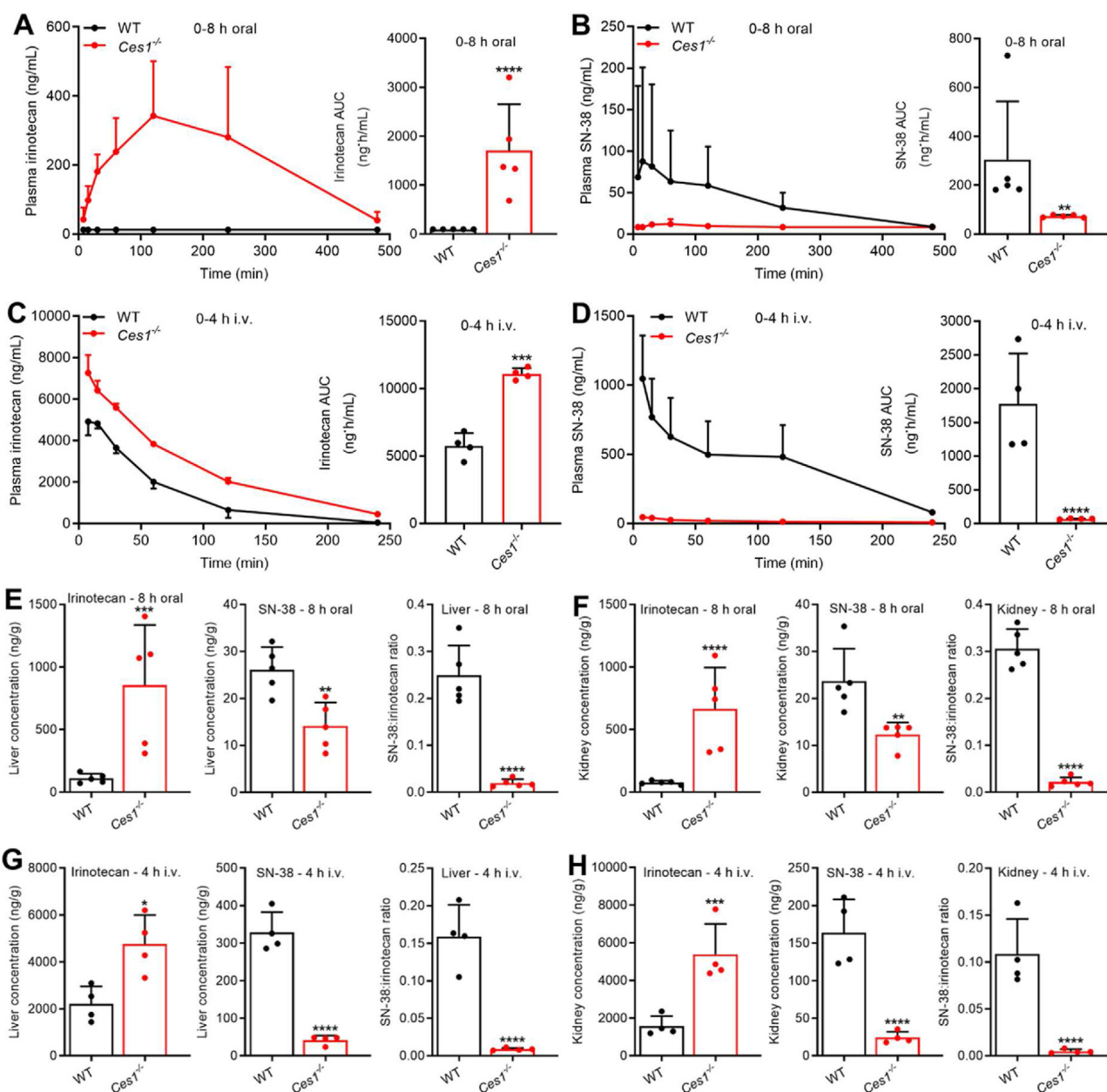
Figure 2 Ces1 loss strongly reduces irinotecan conversion to SN-38. Pharmacokinetics of irinotecan and SN-38 after oral or i.v. administration of irinotecan hydrochloride trihydrate (20 mg/kg) to male WT and $Ces1^{-/-}$ mice. Plasma concentration *versus* time curves and AUCs of irinotecan and SN-38 after oral (A, B) or i.v. (C, D) administration of irinotecan. Tissue concentrations of irinotecan, SN-38 and SN-38-to-irinotecan ratios in liver (E, G) and kidney (F, H). Data are presented as mean $\pm$ SD ($n = 4-5$; *$P < 0.05$; **$P < 0.01$; ***$P < 0.001$; ****$P < 0.0001$ when compared with WT mice; the statistical calculation was performed after log-transformation of data; two-tailed unpaired Student's *t* test).

i.v. administration the much higher amount of irinotecan in plasma was more modestly affected by the removal of Ces1 activity (1.9-fold increase, Fig. 2C). Systemic plasma AUCs of SN-38 in $Ces1^{-/-}$ mice were at most 24% or 4% of those seen in WT controls after oral and i.v. administration, respectively (Fig. 2B, D and Table S3). SN-38 was below the limit of detection (8.5 ng/mL) at almost all time points after oral dosing in $Ces1^{-/-}$ mice (Fig. 2B), and vastly reduced after i.v. dosing (Fig. 2D), indicating a pronounced reduction of SN-38 formation in $Ces1^{-/-}$ compared to WT mice.

In liver, the SN-38-to-irinotecan ratio was substantially lower in $Ces1^{-/-}$ mice both after oral and i.v. administration, mainly because of a higher absolute concentration of irinotecan and a

lower SN-38 concentration (Fig. 2E and G). A similar profile was seen in kidney (Fig. 2F and H). Spleen and lung also showed significantly lower SN-38-to-irinotecan ratios in $Ces1^{-/-}$ mice both after oral and i.v. dosing (Supporting Information Fig. S2), and similar differences in absolute drug concentrations between WT and $Ces1^{-/-}$ mice as liver and kidney, especially after i.v. administration (Fig. S2C and S2D). Given the prominent impact of Ces1 on the plasma levels of irinotecan and SN-38, it is difficult to cleanly distinguish the tissue-specific and plasma-specific contribution of Ces1 to the conversion from irinotecan to SN-38. We note that mouse Ces1c, unlike human CES1, is an abundant plasma enzyme. Consequently, it will have a strong impact on the conversion of any irinotecan present in plasma to SN-38, as the

irinotecan is continually exposed to the plasma Ces1c. This SN-38 in plasma may then readily distribute from plasma to all tissues. However, as neither tissue-to-plasma ratios nor tissue accumulation parameters were identical between the two strains (Supporting Information Fig. S3), it seems likely that the tissue concentrations did not simply reflect the plasma concentrations of the compounds. We also measured the small intestine tissue, small intestinal content (SIC) and colon levels of irinotecan and SN-38. Clear decreases in SN-38-to-irinotecan ratios showed up in most cases in $Ces1^{-/-}$ mice, except for SIC-oral and colon-i.v. (Supporting Information Fig. S4C and S4F). However, also due to high interindividual variation, we rarely observed significant differences in absolute concentrations or recovered amounts of irinotecan and SN-38 among these three compartments between WT and $Ces1^{-/-}$ mice. Compared to all other tissues analyzed, high concentrations of both irinotecan and SN-38 were seen in the SIC of WT mice, especially after i.v. administration (Fig. S4D), illustrating the extensive capacity for excreting these compounds into the intestinal lumen.

Mouse Ces2 can also hydrolyze irinotecan, and these enzymes are most likely responsible for the residual level of SN-38 formation that was observed in plasma and all analyzed tissues. However, likely the prominent role of plasma Ces1c in conversion of irinotecan to SN-38 in plasma has resulted in a comparatively disproportionate impact of Ces1 on the overall pharmacokinetics of irinotecan and SN-38 in mice.

3.3. Stable liver-specific expression of human CES1 in transgenic mice of Ces1 knockout background

To investigate the possible roles of human CES1 *in vivo*, we aimed to generate human CES1 transgenic mice with stable and liver-specific expression by zygote injection of an ApoE promoter-HCR1 driven expression cassette[26], containing wild-type human CES1 cDNA (Fig. 3A). The transgene was then crossed into a $Ces1^{-/-}$ background and bred to homozygosity for the transgene and knockout alleles to obtain humanized TgCES1 mice. Western blot analysis of crude membrane proteins of liver, small intestine and kidney showed that CES1 was abundantly expressed in the liver of male and female TgCES1 mice (Fig. 3B). No CES1 expression was observed in the small intestine of this strain, but the transgene was slightly expressed in the kidney of TgCES1 male mice. These Western blot results were confirmed by immunohistochemical staining, which showed strong hepatic CES1 expression, especially in periportal areas of TgCES1 male mice, but no intestinal staining (Fig. 3C and Supporting Information Fig. S5A). In the kidney of TgCES1 male mice, focused CES1 staining in proximal tubule epithelial cells and Bowman's capsule was observed (Fig. S5B). A similar localization was previously seen for human OATP1B1/3 overexpression driven by the ApoE-HCR1 expression cassette[26]. No CES1 expression was detected in white and brown adipose tissues (Fig. S5C). We observed a quite comparable human CES1 expression pattern in TgCES1 females (data not shown). Hepatic expression of transgenic CES1 was monitored over approximately 8 generations and was found to be stable (data not shown). Unlike mouse Ces1c, human CES1 will not be secreted into plasma as it contains an endoplasmic reticulum retention signal.

RT-PCR analysis of potential *Ces2* gene expression changes in the $Ces1^{-/-}$ and TgCES1 mouse strains revealed no significant or meaningful changes in male and female liver or male small intestine (Supporting Information Fig. S6A−S6F). Only in female

$Ces1^{-/-}$ small intestine we observed significant, about 2-fold upregulation of the *Ces2a*, *2b*, and *2c* genes, which was reversed in the TgCES1 mice (Fig. S6G and S6H). Considered in the context of the substantial pharmacokinetic and physiological changes we observed in these mouse strains (see also below) it seems unlikely that these modest shifts in female small intestine would have had a strong impact on those changes.

3.4. Human CES1 transgenic mice show increased formation of SN-38 from irinotecan in liver and kidney

In vitro, human CES2 appears to hydrolyze irinotecan more efficiently (> 50-fold) than human CES1[28]. Yet, about 50% of hepatic irinotecan hydrolysis is thought to be mediated by human CES1 because of its high and predominant expression in liver. In the clinic, irinotecan is intravenously administered to patients, so the question arises to what extent human CES1 can impact irinotecan metabolism in an intact animal model. To explore this, we analyzed irinotecan and SN-38 pharmacokinetics in TgCES1, WT and $Ces1^{-/-}$ mice. After intravenous administration of 20 mg/kg irinotecan hydrochloride trihydrate, at 7.5 and 15 min, we observed moderately but significantly higher SN-38-to-irinotecan ratios in plasma of TgCES1 compared to $Ces1^{-/-}$ mice, but not at later time points (Fig. 4A). This suggests a modest role for hepatic human CES1 in the plasma disposition of irinotecan and SN-38 at early time points. The overall SN-38-to-irinotecan AUC ratios were similar between $Ces1^{-/-}$ and TgCES1 mice, and markedly lower than in WT (Fig. 4B). No significant differences in absolute plasma concentrations of irinotecan and SN-38 were observed between TgCES1 and $Ces1^{-/-}$ mice, nor for plasma AUCs of irinotecan and SN-38 (Supporting Information Fig. S7A and S7B). These data indicate that hepatic human CES1 has only a minor impact on i.v. irinotecan and SN-38 metabolism and disposition in the plasma compartment. In contrast, with respect to liver and kidney, while irinotecan concentrations were similar between $Ces1^{-/-}$ and TgCES1 mice (Fig. 4C and F), the SN-38 concentrations in TgCES1 mice were increased to the same levels as seen in WT mice (Fig. 4D and G). Accordingly, the SN-38-to-irinotecan ratios in these tissues in TgCES1 were much higher than in $Ces1^{-/-}$ mice (Fig. 4E and H), albeit still slightly lower than in WT mice. Similar shifts were observed for SN-38 concentration (Fig. 4D and G) and fraction of dose (Fig. S7D and S7F), with TgCES1 values roughly equaling WT values. Pooling of the WT and $Ces1^{-/-}$ data of the i.v. experiments in Figs. 2 and 4 resulted in very similar results ($n = 7−9$), with statistical significance of all tested differences at least as high as seen in the graphs of Fig. 4 (data not shown).

These results indicate that expression of human CES1 in liver and kidney can markedly increase the local irinotecan to SN-38 conversion. They also confirm that the transgenic CES1 is enzymatically active. The absence of marked effects of TgCES1 on the plasma disposition of irinotecan and SN-38 suggests that the strong changes between WT and $Ces1^{-/-}$ mice there are mainly caused by the mouse plasma-localized Ces1c enzyme. We also assessed other tissues not expressing transgenic CES1 (spleen, lung, SI, SIC and colon) but no clear differences between $Ces1^{-/-}$ and TgCES1 mice were observed (data not shown). This suggests that the shifts were restricted to tissues expressing human CES1.

3.5. Ces1 deficiency reduces WBC and thymus toxicity

In a small-scale toxicity experiment, with 6 once-daily i.v. irinotecan injections at a dose (30 mg/kg) that should cause only
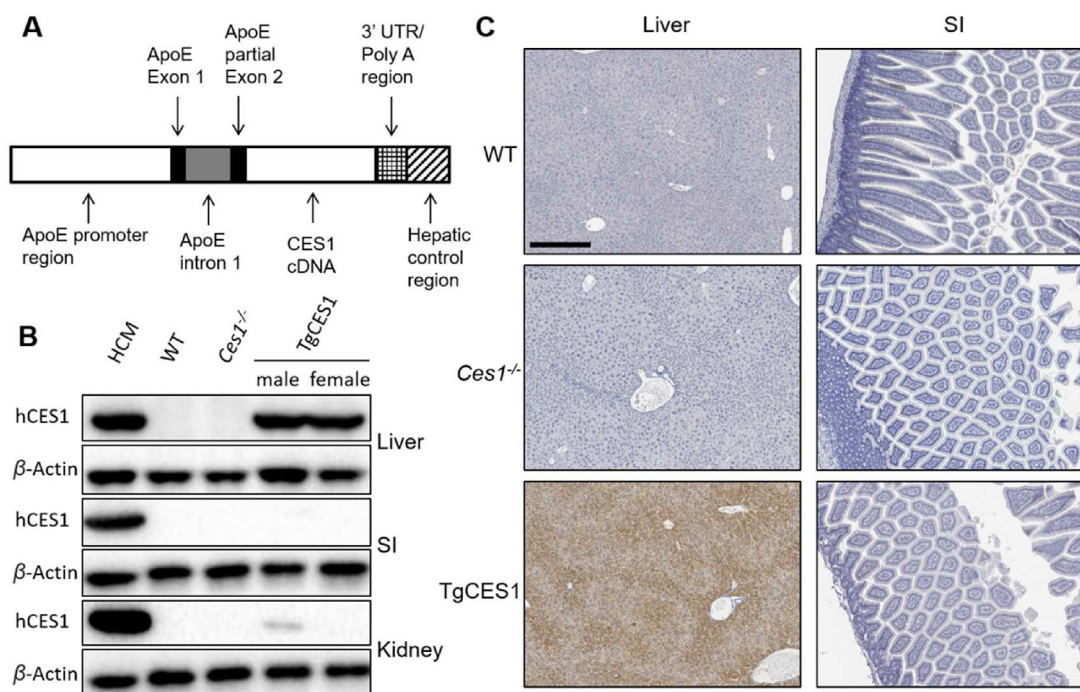
Figure 3 Human CES1 expression in transgenic mice. (A) Schematic structure of the ApoE promoter-HCR1-driven expression cassette containing wild-type human *CES1* cDNA. (B) Western blot analysis of crude membrane protein of liver, small intestine (SI) and kidney from WT, *Ces1*^{−/−} and TgCES1 mice. Crude membrane protein from human liver (HCM) was used as positive control. HCM: human crude liver membrane. (C) Immuno-histochemical staining of human CES1 in liver and small intestine of WT, *Ces1*^{−/−} and TgCES1 male mice. Scale bar: 300 μm.

limited toxicity in WT mice, we observed similar mild body-weight loss (∼7% over 7 days) between WT, *Ces1*^{−/−} and TgCES1 mice (Supporting Information Fig. S8A). However, while the number of white blood cells (WBC) was significantly reduced in WT and TgCES1 mice (Day 7 compared to Day 0), in *Ces1*^{−/−} mice there was no significant shift, although the differences were small (Fig. S8B). More strikingly, histopathology on Day 7 revealed that the WT mice showed dramatic thymus atrophy (lymphocytic depletion, with extensive thinning of cortex and medulla leading to a very small size of the thymus) compared with a much more normal-looking thymus in *Ces1*^{−/−} mice, whereas TgCES1 mice suffered only a moderate depletion of the thymus cortex (Fig. S8C). In contrast, the structure of the jejunum and cell density of sternal bone marrow appeared relatively normal in these 3 mouse strains, consistent with only mild bodyweight loss (Fig. S8D and S8E). These results suggest that the lower systemic SN-38 exposure in *Ces1*^{−/−} and TgCES1 mice resulted in reduced irinotecan/SN-38 toxicity in these strains with respect to the thymus, whereas transgenic CES1 could partially revert this relative resistance in thymus and WBC.

3.6. Mouse Ces1 and human CES1 influence metabolite-to-capecitabine ratios in plasma

Capecitabine is an oral fluoropyrimidine (5-FU) carbamate pro-drug for treatment of metastatic breast and colorectal cancer[24]. *In vitro*, both human CES1 and CES2 can hydrolyze the carbamate bond in capecitabine to yield its first metabolite, 5-DFCR, with roughly equal efficiency (Supporting Information Scheme S2). We administered 500 mg/kg capecitabine by oral gavage to female WT, *Ces1*^{−/−} and TgCES1 mice. HPLC−MS/MS was used to measure the levels of capecitabine and 4 of its metabolites

(5-DFCR, 5-DFUR, 5-FU and FBAL)[24]. We observed a 63.4-fold higher plasma AUC of capecitabine in *Ces1*^{−/−} *versus* WT. The plasma AUC of capecitabine in TgCES1 mice was about half that in *Ces1*^{−/−} mice (Supporting Information Fig. S9A and S9B), but still far higher than that in WT mice. Somewhat surprisingly, the absolute values of plasma AUCs for the 4 metabolites (5-DFCR, 5-DFUR, 5-FU and FBAL) were similar among all three strains (Fig. S9C−S9J). Still, the dynamic conversion from capecitabine to 5-DFCR, as calculated by the 5-DFCR-to-capecitabine ratio in plasma, was clearly impacted by mouse Ces1 and human hepatic CES1. In *Ces1*^{−/−} mice, the plasma AUC ratio of 5-DFCR-to-capecitabine was 98.9% lower than that in WT mice, and a 2.2-fold increase in AUC ratio was observed in TgCES1 compared to *Ces1*^{−/−} mice (Fig. 5A and B). Similar tendencies of differences were detected for the metabolite-to-capecitabine ratios of the other three metabolites, although these were mainly driven by the shifts in plasma capecitabine concentrations (Fig. 5C−H and Supporting Information Table S4). Together, these data demonstrate that mouse Ces1 and hepatic human CES1 enzymes can influence the pharmacokinetics of capecitabine and related metabolites in plasma. There were no significant differences between the three strains (neither for absolute concentrations, nor for ratios) in various tissues analyzed (liver, kidney, spleen, lung, SI, SIC and colon) (data not shown). It is worth noting that capecitabine is an oral prodrug of 5-FU, which itself needs to be further metabolized intracellularly to exert its anticancer action. However, despite the clear impact of Ces1/CES1 on plasma levels of capecitabine, the 5-FU concentrations in plasma and tissues were not significantly altered in the knockout and transgenic strains (Fig. S9G and S9H and data not shown). Apparently, there are sufficient alternative conversion routes to still generate similar amounts of 5-DFUR and 5-FU in the absence of Ces1/CES1.
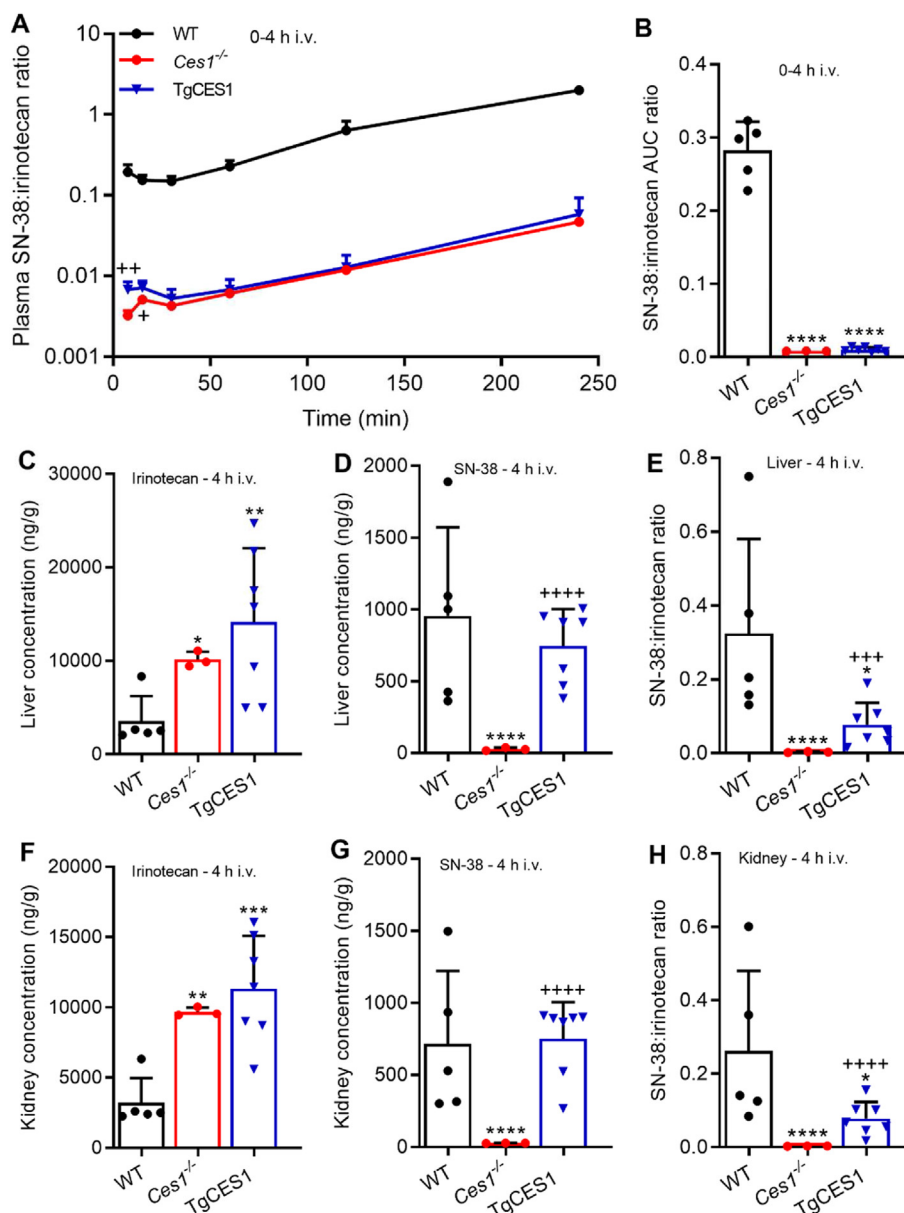
Figure 4 Human CES1 transgenic mice exhibit enhanced metabolism of irinotecan to SN-38 in liver and kidney. Pharmacokinetics of irinotecan and SN-38 after i.v. administration of irinotecan hydrochloride trihydrate (20 mg/kg) to male WT, $Ces1^{-/-}$ and TgCES1 mice. (A, B) Plasma SN-38-to-irinotecan ratio *versus* time curves and AUC ratios. Tissue concentrations of irinotecan, SN-38 and SN-38-to-irinotecan ratios in liver (C–E) and kidney (F–H). Data are presented as mean ± SD ($n = 3–7$; *$P < 0.05$; **$P < 0.01$; ***$P < 0.001$; ****$P < 0.0001$ when compared with WT mice; +$P < 0.05$; ++$P < 0.01$; +++$P < 0.001$; ++++$P < 0.0001$ when TgCES1 compared with $Ces1^{-/-}$ mice; the statistical calculation was performed after log-transformation of data; one-way ANOVA followed by Tukey's *post hoc* test).

3.7. Ces1 deficiency results in increased body weight, disrupted lipid homeostasis and hepatic expression of human CES1 reverses these phenotypes

The entire *Ces1* cluster knockout and hepatic human CES1 transgenic mice we generated present unique tools to better study the physiological functions of the mouse Ces1 and human CES1 enzymes. We initially compared body weights at around 12–13 weeks of age among WT, $Ces1^{-/-}$ and TgCES1 mice fed a standard medium-fat diet. $Ces1^{-/-}$ mice showed significantly higher body weights than the WT strain. Importantly, the TgCES1 mice showed marked reduction of the increased body weights in $Ces1^{-/-}$ mice (Supporting Information Fig. S10A).

We next monitored the body weight development for males from 6 to 15 weeks. Starting from 6 weeks of age, $Ces1^{-/-}$ mice showed higher body weights than their WT littermates. TgCES1 mice displayed moderately but significantly reduced body weights compared with $Ces1^{-/-}$ mice, which was confirmed by AUC data (Fig. 6A). As to the origin of these weight differences, dissection of mice at 12–13 weeks revealed that $Ces1^{-/-}$ mice had markedly elevated weights of the inguinal white adipose tissue (iWAT), mesenteric white adipose tissue (mWAT), and interscapular brown adipose tissue (iBAT), but not for perigonadal white adipose tissue (gWAT) and retroperitoneal white adipose tissue (rWAT)[29]. Interestingly, the weights of iWAT and mWAT depots as well as iBAT were significantly reduced again in TgCES1 mice (Fig. 6B).
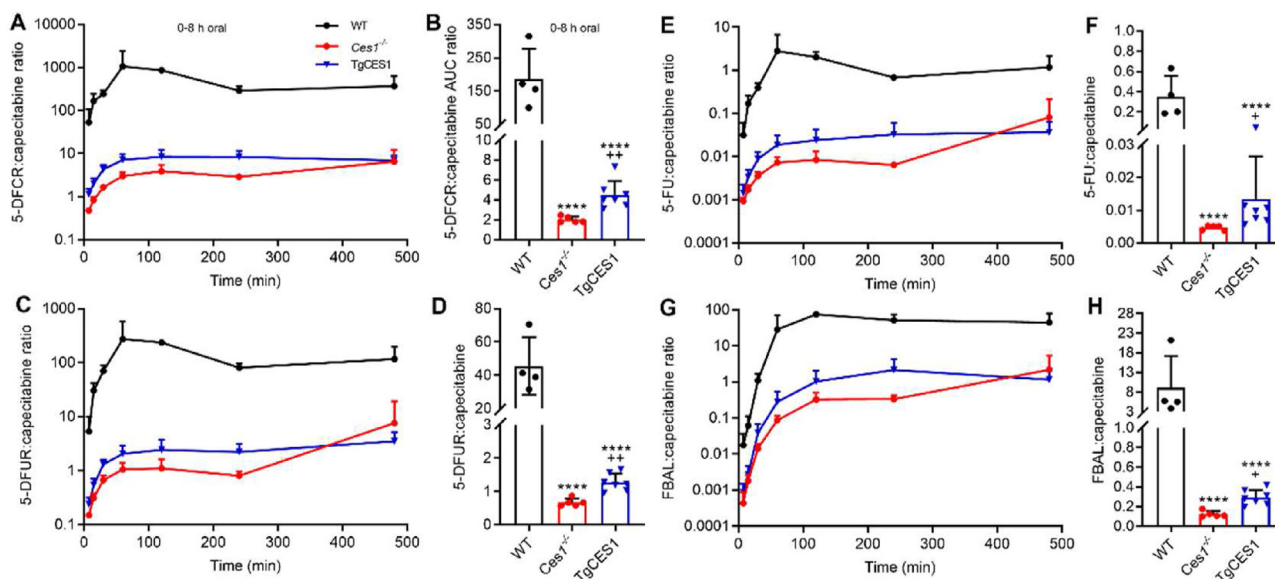
Figure 5 Mouse Ces1 and human CES1 influence metabolite-to-capecitabine ratios in plasma. Pharmacokinetics of capecitabine and its 4 metabolites (5-DFCR, 5-DFUR, 5-FU and FBAL) after oral administration of capecitabine (500 mg/kg) to female WT, $Ces1^{-/-}$ and TgCES1 mice. (A, B) Plasma 5-DFCR to capecitabine ratio *versus* time curves and AUC ratios. (C, D) Plasma 5-DFUR to capecitabine ratio *versus* time curves and AUC ratios. (E, F) Plasma 5-FU to capecitabine ratio *versus* time curves and AUC ratios. (G, H) Plasma FBAL to capecitabine ratio *versus* time curves and AUC ratios. Data are presented as mean $\pm$ SD ($n = 4-7$; ****$P < 0.0001$ when compared with WT mice; $^{+}P < 0.05$; $^{++}P < 0.01$ when TgCES1 compared with $Ces1^{-/-}$ mice; the statistical calculation was performed after log-transformation of the data; one-way ANOVA followed by Tukey's *post hoc* test).

Other organ weights were roughly similar among the three strains of mice, and the same applied for liver. But liver to body weight ratio of TgCES1 mice was significantly higher than WT and $Ces1^{-/-}$ mice (Fig. S10B−S10D).

Histological examination by haematoxylin and eosin (H&E) staining revealed that in males gWAT adipocytes from $Ces1^{-/-}$ mice were somewhat larger than those from WT mice, and again reduced in size in TgCES1 mice. Interestingly, gWAT of $Ces1^{-/-}$ mice showed infiltration of immune cells (steatitis), and hepatic expression of human CES1 appeared to protect TgCES1 mice from this inflammatory response. Similar histological examination of iBAT showed that $Ces1^{-/-}$ iBAT had significantly more lipid deposition than WT iBAT, which was mostly reversed in TgCES1 iBAT (Fig. 6C). This suggests that hepatic human CES1 can also impact lipid homeostasis in iBAT. Collectively, these results indicate that deficiency of all mouse Ces1 genes causes increased body weight mainly due to increased WAT mass. These data also provide strong support for a function of hepatic human CES1 in the lipid homeostasis in adipose tissues, reducing overall lipid accumulation in these compartments. Compared to males, females of these three strains manifested very similar differences in body weight development (Supporting Information Fig. S11A) and all 4 isolated white adipose tissues displayed markedly increased weight in $Ces1^{-/-}$ mice, which was reversed in TgCES1 mice (Fig. S11B). Other organ weights (kidney, spleen, lung, and heart) were similar among these three female strains (data not shown). Like in males, H&E staining revealed that $Ces1^{-/-}$ females had larger gWAT adipocytes, and this was to some extent reduced again in TgCES1 females. However, unlike in males, almost no steatitis showed up in $Ces1^{-/-}$ gWAT. Female iBAT showed an increased lipid load in $Ces1^{-/-}$ mice, albeit not as pronounced as in males, and this was again reversed in TgCES1 mice (Fig. S11C). Possibly gender differences in lipid handling by the FVB/NRj mouse strain may play a role here.

To assess possible changes in energy metabolism (heat production) in iBAT as an explanation for the changes in body weight and lipid load in WAT and iBAT in the three mouse strains, we measured the expression of the following thermogenic genes in iBAT: *Ucp1*, *Pgc1a*, *Prdm16*, *Cidea*, *Elovl3* and *Cox8b*, in males and females. None of these genes showed significant changes in expression (Supporting Information Fig. S12). It seems therefore unlikely that there were significant differences in heat production and thus lipid consumption in the iBAT of the three mouse strains.

3.8. Hepatic expression of human CES1 increases triglyceride delivery from liver to plasma in mice

We observed notably higher free fatty acid and triglyceride concentrations in plasma of TgCES1 compared to both $Ces1^{-/-}$ and WT male mice (Supporting Information Fig. S13D and Fig. 7A). We therefore further explored if there is altered triglyceride secretion in our newly generated mouse models. In a triglyceride production assay, a slightly but significantly higher plasma triglyceride level was detected in TgCES1 compared with WT and $Ces1^{-/-}$ strains, as also confirmed by AUC data (Fig. 7B). The hepatic delivery of triglyceride to blood plays an important role in the triglyceride balance between liver, blood, and the rest of the body[30]. Since we observed higher triglyceride in plasma, plus increased triglyceride production from liver to plasma in TgCES1 mice, we tested the triglyceride level in the liver. Similar liver weights were observed (Fig. S10C), but TgCES1 mice possessed markedly higher triglyceride concentrations in liver than $Ces1^{-/-}$ and WT mice (Fig. 7C). The lipid contents of livers were further confirmed by Oil Red O (ORO) staining. Histological examination by H&E staining also suggested slightly more unstained lipid-like structures in TgCES1 liver (Fig. 7D).

In females, the triglyceride level in plasma of TgCES1 mice was also markedly higher than that in $Ces1^{-/-}$ and WT mice, but
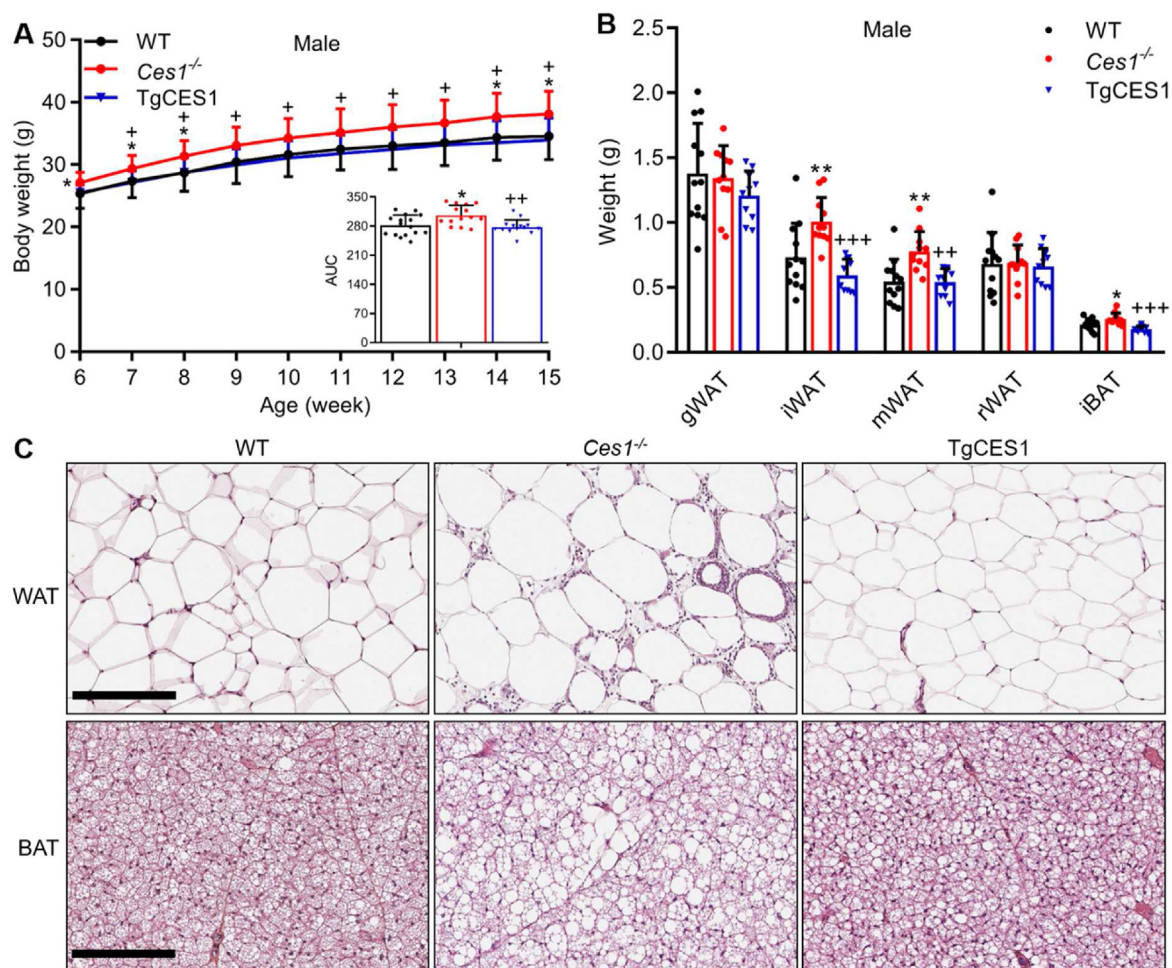
Figure 6 Ces1 deficiency results in increased body weight, disrupted lipid homeostasis and hepatic expression of human CES1 reverses these phenotypes in male mice. Male WT, $Ces1^{-/-}$ and TgCES1 mice on a medium-fat diet were analyzed. (A) Body weight-time curves between 6 and 15 weeks of age, with inset showing the area under the curves ($n = 14-16$). (B) Weight of different adipose tissue depots ($n = 10-12$, $12-13$ weeks). (C) Haematoxylin and eosin staining of perigonadal white adipose tissue (top panels) and brown adipose tissue (bottom panels) ($n = 10-12$, $12-13$ weeks). Scale bar: 200 μm. Data are presented as mean ± SD (*$P < 0.05$; **$P < 0.01$ when $Ces1^{-/-}$ compared with WT mice; +$P < 0.05$; ++$P < 0.01$; +++$P < 0.001$ when TgCES1 compared with $Ces1^{-/-}$ mice; one-way ANOVA followed by Tukey's *post hoc* test).

plasma glycerol and free fatty acid levels were similar (Supporting Information Figs. S14A, S13A and S13B). TgCES1 females also displayed stronger hepatic triglyceride production than $Ces1^{-/-}$ and WT mice (Fig. S14B). However, hepatic triglyceride concentrations of these strains were comparable, albeit with high variation (Fig. S14C). Whereas the liver weight in TgCES1 was higher than in $Ces1^{-/-}$ and WT, and $Ces1^{-/-}$ mice showed lower liver to body weight ratio than in WT control, the liver to body weight ratio in TgCES1 was much higher than in the other two strains (Fig. S14D and S14E). H&E staining in TgCES1 female liver also showed more unstained lipid-like structures than in $Ces1^{-/-}$ and WT females, or TgCES1 males, and the staining level of hepatic lipid content by ORO appeared to be slightly higher in the female TgCES1 mice than in the other two strains (Fig. S14F).

Since the triglyceride plasma data suggested a possibly higher net triglyceride synthesis in the TgCES1 strain, we tested by RT-PCR the RNA expression of two panels of genes involved in hepatic fatty acid and triglyceride synthesis, respectively. Across males and females, we found similar profiles of increased expression of four genes involved in fatty acid synthesis in TgCES1 mice (*Fasn*, *Acc1*, *Acc2*, and *Srebp1c*) (Fig. 7E and Fig. S14G), which became even more clear-cut after pooling of male and female data (Supporting Information Fig. S15). For triglyceride synthesis only one gene was significantly increased in TgCES1 female mice, *Gpam* (Supporting Information Fig. S16). Altogether, these data are compatible with possibly overall increased hepatic fatty acid and thus also triglyceride synthesis in the TgCES1 strain.

3.9. Glucose and insulin tolerance tests in WT, $Ces1^{-/-}$ and TgCES1 mice

Disrupted lipid homeostasis may lead to impaired glucose homeostasis, as previously observed in several Ces1/CES1 genetically modified mouse models[21,22,31,32]. In oral glucose tolerance test (GTT), $Ces1^{-/-}$ mice had markedly higher fasting blood concentrations of glucose, whereas the blood glucose levels were significantly reduced again in TgCES1 mice compared with the $Ces1^{-/-}$ controls. After glucose administration, $Ces1^{-/-}$ mice

showed higher blood glucose levels, and the blood glucose levels in TgCES1 mice roughly reverted back to the WT control values (Fig. 8A). This was confirmed by the AUC data (Fig. 8B). In the insulin tolerance test (ITT), the responses to insulin challenge in the three strains were similar, albeit with high variation. Even though at 15 and 30 min significantly higher blood glucose levels were detected in $Ces1^{-/-}$ mice (Fig. 8C), the AUC data were comparable between the three strains (Fig. 8D). The data suggest that, under a medium-fat diet, the mouse Ces1 and human CES1 enzymes can positively affect glucose metabolism in the glucose tolerance test, but the response to insulin is more limited. We also performed GTT and ITT in female mice as described above for males. In the GTT, differences in fasting blood glucose levels were similar to those in males, with $Ces1^{-/-}$ values clearly higher than in the other two strains. After glucose administration, at late time points (90 and 120 min) higher blood glucose levels were observed in $Ces1^{-/-}$ mice compared to WT (Supporting Information Fig. S17A), but TgCES1 values were not reduced again, and the AUC data were comparable between the three female strains (Fig. S17B). In the ITT, TgCES1 females exhibited higher blood glucose than the other two strains (Fig. S17C and S17D), suggesting that the capacity of lowering blood glucose by insulin is moderately hampered in TgCES1 females compared to $Ces1^{-/-}$ and WT controls. Unlike in males, $Ces1^{-/-}$ females showed a relatively strong early response to insulin compared to the other two strains.

4. Discussion

Our results demonstrate that Ces1/CES1 can effectively function as a detoxification system for both xenobiotic and lipid toxins. While not often considered as such, lipids are potential physiological toxins. A general or local excess of lipids can result in severe and even lethal toxic effects, as seen in *e.g.* obesity-related inflammation, non-alcoholic fatty liver disease and atherosclerosis. Type 2 diabetes is another serious downstream toxic effect of lipid overaccumulation. Apparently Ces1/CES1 helps to mobilize these lipids, allowing them to be cleared more easily from cells, and thus reducing their toxicity. In our study this was apparent from increased body weight, adipose tissue lipid accumulation and inflammation, and type 2 diabetes phenotypes upon deletion of *Ces1* genes, that could all be rescued by liver-specific expression of human CES1 in males, and nearly all in females.

Among our newly generated mouse models, $Ces1^{-/-}$ mice displayed a strongly impaired ability to hydrolyze the prodrug irinotecan to the active metabolite SN-38 in plasma and tissues. Hepatic hydrolysis of irinotecan is likely most important in patients as irinotecan is normally intravenously administered, and human CES1 is abundantly expressed in the liver, and not in plasma. This should make our TgCES1 strain a relatively good model to explore the role of hepatic human CES1 in irinotecan/SN-38 metabolism. In human CES1-expressing tissues (liver and kidney), conversion of irinotecan to SN-38 was almost fully rescued to the levels seen in WT mice (Fig. 4C−H and Fig. S7C−S7F), indicating that the transgenic human CES1 has similar hydrolyzing potency for irinotecan as the mouse Ces1 enzymes in these two tissues. Fig. 4D shows that hepatic human CES1 has a huge impact on the amount of SN-38 that is formed in the liver after i.v. irinotecan administration, effecting a 26.9-fold increase. As liver is also the main site of metastases of colorectal cancer, one of the main indications for clinical application of irinotecan, our data suggest that hepatic

CES1 activity might be an important, possibly even crucial effector in the clinical application of irinotecan. Our finding that *Ces1* deficiency reduces the toxicity of irinotecan, at least with respect to WBC and thymus, supports a role of CES1 in enhancing the pharmacodynamic activity of irinotecan. The present study also demonstrates that the mouse Ces1 and human hepatic CES1 enzymes play an important role in the plasma exposure of capecitabine and to a lesser extent 5-DFCR, but have only limited impact on the abundance of the further capecitabine metabolites. The most likely explanation is that there are various other (non-Ces1) esterases in mice that can efficiently mediate conversion of capecitabine into 5-DFCR, especially in tissues such as liver. Overall, these data suggest that, at least in mice, due to a redundancy in capecitabine-hydrolyzing esterases, CES1 activity in itself is not a major determinant of 5-FU exposure. Although speculative, this might well also apply in humans.

It is well established that carboxylesterase 1 family members are involved in lipid metabolism, and can influence development of metabolic disorders such as obesity, atherosclerosis and fatty liver disease[7,21,22,33]. Distinct but at times also contradictory insights into the *in vivo* physiological functions of Ces1/CES1 enzymes have been obtained from single *Ces1* gene knockouts and human CES1 transgenic mouse models in a WT background[21,22]. Eight different mouse *Ces1* genes originating from tandem gene duplication appear to correspond to just one mature human CES1 enzyme[5]. It is therefore difficult, if not impossible, to define whether one or more mouse *Ces1* genes are clear orthologs of the human *CES1*. The generation of a full mouse *Ces1* cluster deletion model and hepatic humanized CES1 mice in this knockout background may therefore yield more appropriate models to investigate physiological functions of the Ces1/CES1 family *in vivo*. *Ces1d* single knockout mice had increased WAT weight accompanied by larger adipocyte size compared with WT[21], just as we observed in $Ces1^{-/-}$ mice. Over-expanded adipocyte cell size is often associated with hypoxia and cell death which can produce pro-inflammatory signaling molecules, attracting immune cell infiltration[34], which had happened in male $Ces1^{-/-}$ WAT (Fig. 6C).

Body weights and adipose tissue weights of TgCES1 males and females reverted to similar levels as seen in WT controls, as was the case for white adipocyte size and lipid loading in BAT. The WAT inflammation seen in $Ces1^{-/-}$ male mice was also relieved in TgCES1 mice (Fig. 6 and Fig. S11). Human CES1 was not detected in WAT or BAT of TgCES1 mice (Fig. S5C). This suggests that hepatic CES1 activity can remotely regulate lipid homeostasis in adipose tissues. We found that triglyceride levels in both plasma and liver compartments were enhanced in TgCES1 male mice relative to both WT and $Ces1^{-/-}$ mice (Fig. 7A and C). HE and ORO staining of male livers confirmed that lipid loading was somewhat higher in TgCES1 than in WT and $Ces1^{-/-}$ liver, although it was still considered within the normal physiological range (Fig. 7D). We also detected increased secretion of triglyceride from liver to plasma in TgCES1 mice (Fig. 7B and Fig. S14B). These results suggest that in TgCES1 mice hepatic CES1 can stimulate triglyceride synthesis in liver and also mobilize its secretion into plasma. Liver is the main distributor of lipids to other organs; triglyceride is incorporated and partitioned into lipoprotein (like VLDL) for secretion, but before that can happen, cytosolically stored triglyceride in liver needs to be hydrolyzed followed by re-esterification in the endoplasmic reticulum[35]. Hepatic human CES1 appears to be one of the enzymes hydrolyzing triglyceride to release substrates for triglyceride re-
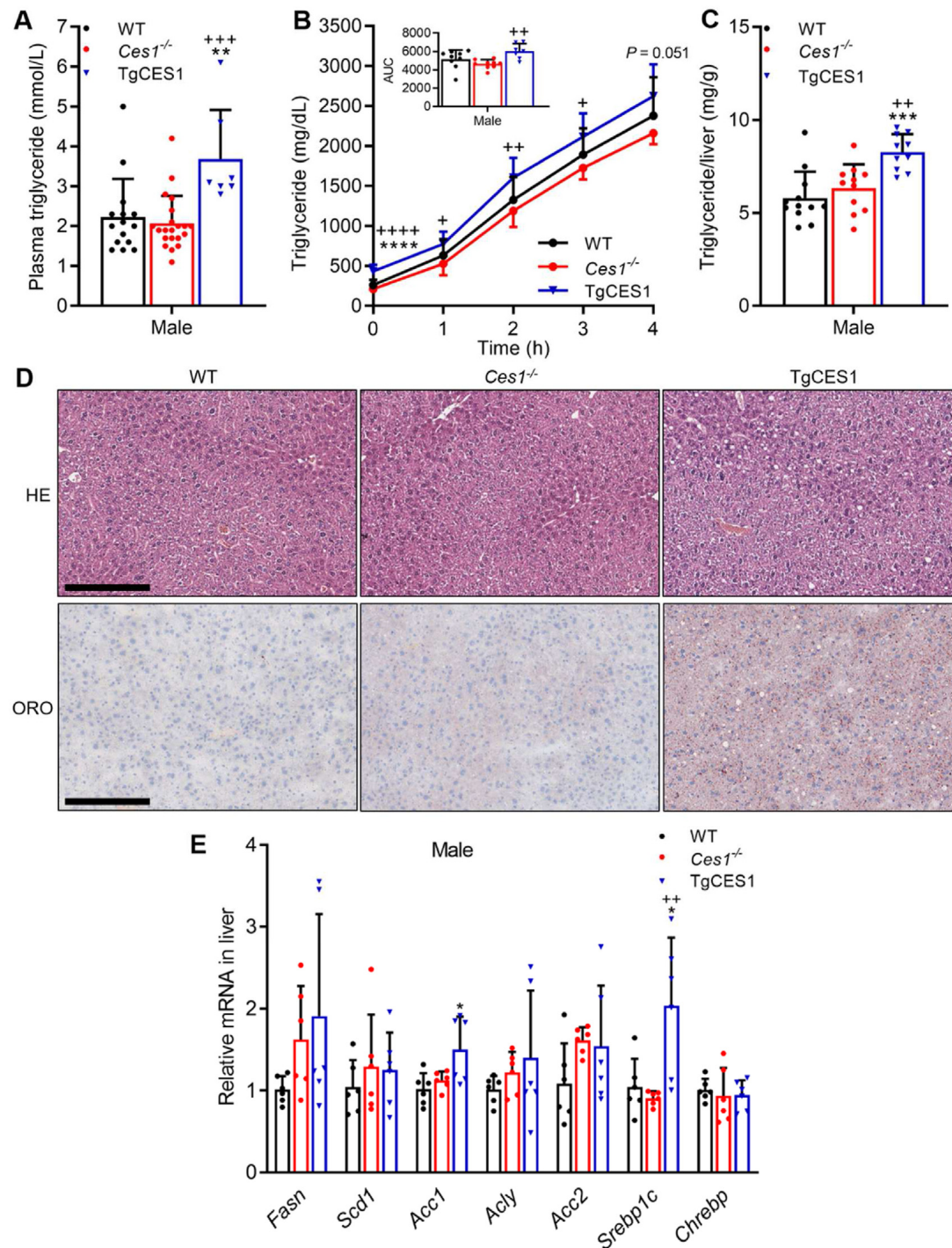
Figure 7 Hepatic expression of human CES1 increases triglyceride secretion from liver to plasma in male mice. (A) Plasma concentration of triglyceride (clinical chemistry analysis) of male mice ($n = 7-21$, 9–16 weeks). (B) Triglyceride secretion from liver to blood. Male mice ($n = 7-9$, 12–14 weeks) were i.p. injected with lipase inhibitor P-407, plasma was collected and measured at indicated time points. (C) Triglyceride concentration in liver ($n = 10-12$, 12–13 weeks). (D) Haematoxylin and eosin (top panels), Oil Red O (bottom panels) staining of liver ($n = 8-12$, 12–13 weeks). Scale bar: 200 μm. (E) RT-PCR analysis of fatty acid synthesis genes in liver ($n = 6$, 12–13 weeks). Data are presented as mean $\pm$ SD (*$P < 0.05$; **$P < 0.01$; ***$P < 0.001$; ****$P < 0.0001$ when TgCES1 compared with WT mice; +$P < 0.05$; ++$P < 0.01$; +++$P < 0.001$; ++++$P < 0.0001$ when TgCES1 compared with $Ces1^{-/-}$ mice; one-way ANOVA followed by Tukey's *post hoc* test).

esterification and thus stimulating hepatic triglyceride secretion[36]. We envisage that in TgCES1 mice, the involvement of hepatic human CES1 in the hydrolysis-re-esterification process may mobilize and utilize more triglyceride, which improves global lipid homeostasis, but at the cost of higher triglyceride in liver itself of TgCES1 male mice. Consequently, the WAT lipid burden is alleviated as reflected by smaller adipocyte size, disappearing inflammation in male WAT, and lower lipid load in BAT in
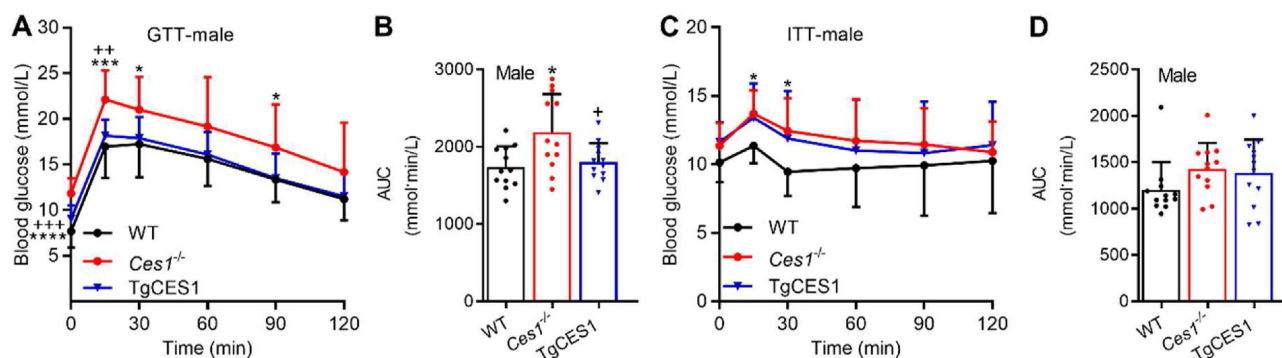
Figure 8 Glucose and insulin tolerance tests in male WT, $Ces1^{-/-}$ and TgCES1 mice. (A, B) Male mice were fasted for 16 h, glucose (1 mg/g) was orally administered ($n = 12$, $11-12$ weeks), and blood glucose was measured. (C, D) Male mice were fasted for 6 h, insulin (0.5 U/kg) was i.p. administered ($n = 12$, $11-12$ weeks), and blood glucose was measured. Data are presented as mean $\pm$ SD ($*P < 0.05$; $***P < 0.001$; $****P < 0.0001$ when $Ces1^{-/-}$ compared with WT mice; $^{+}P < 0.05$; $^{++}P < 0.01$; $^{+++}P < 0.001$ when TgCES1 compared with $Ces1^{-/-}$ mice; one-way ANOVA followed by Tukey's *post hoc* test).

TgCES1 mice (Fig. 6C and Fig. S11C). Somewhat surprisingly, the triglyceride mobilization and liver morphology of $Ces1^{-/-}$ and WT mice were quite similar. This may possibly originate from compensatory effects of different Ces enzymes.

5. Conclusions

We demonstrated that mouse Ces1 and human CES1 are strongly involved in the *in vivo* metabolism of irinotecan to SN-38 and of capecitabine. They also increased irinotecan toxicity, likely by enhancing the formation of SN-38. We further showed that mouse Ces1 deficiency caused overweight and higher adipose tissue lipid load, and especially in males white adipose tissue inflammation and impaired glucose tolerance. Human CES1 expression in liver could mostly reverse these phenotypes, and it also increased triglyceride secretion into plasma. These results indicate that the carboxylesterase 1 family plays essential roles in drug and lipid metabolism and detoxification. We anticipate that more insights into the *in vivo* roles of Ces1/CES1 enzymes in drug metabolism and in lipid and glucose homeostasis will be obtained from these mouse models, giving impetus to further understanding of pharmacokinetics and of the metabolic syndrome.

Author contributions

Alfred H. Schinkel and Changpei Gan conceived the project, designed the experiments, analyzed the data, and wrote the manuscript. Changpei Gan, Jing Wang and Yaogeng Wang performed mouse experiments and analyzed the data. Alejandra Martínez-Chávez and Michel Hillebrand analyzed mouse samples of irinotecan study. Niels de Vries and Joke Beukers analyzed mouse samples of capecitabine study. Hilde Rosing and Jos H. Beijnen supervised the bioanalytical part of the drug studies. Els Wagenaar, Rahmen Bin Ali, Colin Pritchard and Ivo Huijbers generated the mouse models. Els Wagenaar and Changpei Gan characterized the mouse models. Maria C. Lebre organized reagents and mice, contributed to experiments design and data interpretation. Sjoerd Klarenbeek performed pathology analysis, contributed to data interpretation. All authors reviewed and approved the manuscript.

Conflicts of interest

The authors declare that they have no conflict of interest.

Appendix A.   Supporting information

Supporting data to this article can be found online at https://doi.org/10.1016/j.apsb.2022.10.017.

References

1. Long JZ, Cravatt BF. The metabolic serine hydrolases and their functions in mammalian physiology and disease. *Chem Rev* 2011;**111**: 6022−63.
2. Wang D, Zou L, Jin Q, Hou J, Ge G, Yang L. Human carboxylesterases: a comprehensive review. *Acta Pharm Sin B* 2018;**8**: 699−712.
3. Jin Q, Song LL, Ding LL, Zhang J, Wang DD, Song YQ, et al. High-throughput optical assays for sensing serine hydrolases in living systems and their applications. *TrAC, Trends Anal Chem* 2022:116620.
4. Jin Q, Wu J, Wu Y, Li H, Finel M, Wang D, et al. Optical substrates for drug-metabolizing enzymes: recent advances and future perspectives. *Acta Pharm Sin B* 2022;**12**:1068−99.
5. Holmes RS, Wright MW, Laulederkind SJ, Cox LA, Hosokawa M, Imai T, et al. Recommended nomenclature for five mammalian carboxylesterase gene families: human, mouse, and rat genes and proteins. *Mamm Genome* 2010;**21**:427−41.
6. Fukami T, Yokoi T. The emerging role of human esterases. *Drug Metab Pharmacokinet* 2012;**27**:466−77.
7. Lian J, Nelson R, Lehner R. Carboxylesterases in lipid metabolism: from mouse to human. *Protein Cell* 2018;**9**:178−95.
8. Jones RD, Taylor AM, Tong EY, Repa JJ. Carboxylesterases are uniquely expressed among tissues and regulated by nuclear hormone receptors in the mouse. *Drug Metab Dispos* 2013;**41**:40−9.

9. Wang DD, Zou LW, Jin Q, Guan XQ, Yu Y, Zhu YD, et al. Bioluminescent sensor reveals that carboxylesterase 1A is a novel endoplasmic reticulum-derived serologic indicator for hepatocyte injury. *ACS Sens* 2020;**5**:1987−95.

10. Zhang J, Wang D, Zou L, Xiao M, Zhang Y, Li Z, et al. Rapid bioluminescence assay for monitoring rat CES1 activity and its alteration by traditional Chinese medicines. *J Pharm Anal* 2020;**10**:253−62.

11. Nagashima S, Yagyu H, Takahashi N, Kurashina T, Takahashi M, Tsuchita T, et al. Depot-specific expression of lipolytic genes in human adipose tissues—association among CES1 expression, triglyceride lipase activity and adiposity. *J Atheroscler Thromb* 2011;**18**: 190−9.

12. Jernås M, Olsson B, Arner P, Jacobson P, Sjöström L, Walley A, et al. Regulation of carboxylesterase 1 (CES1) in human adipose tissue. *Biochem Biophys Res Commun* 2009;**383**:63−7.

13. Friedrichsen M, Poulsen P, Wojtaszewski J, Hansen PR, Vaag A, Rasmussen HB. Carboxylesterase 1 gene duplication and mRNA expression in adipose tissue are linked to obesity and metabolic function. *PLoS One* 2013;**8**:e56861.

14. Her L, Zhu HJ. Carboxylesterase 1 and precision pharmacotherapy: pharmacogenetics and nongenetic regulators. *Drug Metab Dispos* 2020;**48**:230−44.

15. Wei E, Gao W, Lehner R. Attenuation of adipocyte triacylglycerol hydrolase activity decreases basal fatty acid efflux. *J Biol Chem* 2007; **282**:8027−35.

16. Okazaki H, Igarashi M, Nishi M, Tajima M, Sekiya M, Okazaki S, et al. Identification of a novel member of the carboxylesterase family that hydrolyzes triacylglycerol: a potential role in adipocyte lipolysis. *Diabetes* 2006;**55**:2091−7.

17. Schreiber R, Taschler U, Wolinski H, Seper A, Tamegger SN, Graf M, et al. Esterase 22 and beta-glucuronidase hydrolyze retinoids in mouse liver. *J Lipid Res* 2009;**50**:2514−23.

18. Wei E, Alam M, Sun F, Agellon LB, Vance DE, Lehner R. Apolipoprotein B and triacylglycerol secretion in human triacylglycerol hydrolase transgenic mice. *J Lipid Res* 2007;**48**:2597−606.

19. Bie J, Wang J, Yuan Q, Kakiyama G, Ghosh SS, Ghosh S. Liver-specific transgenic expression of cholesteryl ester hydrolase reduces atherosclerosis in *Ldlr*$^{-/-}$ mice. *J Lipid Res* 2014;**55**:729−38.

20. Morton CL, Wierdl M, Oliver L, Ma MK, Danks MK, Stewart CF, et al. Activation of CPT-11 in mice: identification and analysis of a highly effective plasma esterase. *Cancer Res* 2000;**60**:4206−10.

21. Wei E, Ben Ali Y, Lyon J, Wang H, Nelson R, Dolinsky VW, et al. Loss of TGH/Ces3 in mice decreases blood lipids, improves glucose tolerance, and increases energy expenditure. *Cell Metab* 2010;**11**: 183−93.

22. Quiroga AD, Li L, Trötzmüller M, Nelson R, Proctor SD, Köfeler H, et al. Deficiency of carboxylesterase 1/esterase-X results in obesity, hepatic steatosis, and hyperlipidemia. *Hepatology* 2012;**56**: 2188−98.

23. Martínez-Chávez A, Rosing H, Gan C, Wang Y, Schinkel AH, Beijnen JH. Bioanalytical method for the simultaneous quantification of irinotecan and its active metabolite SN-38 in mouse plasma and tissue homogenates using HPLC-fluorescence. *J Chromatogr B Analyt Technol Biomed Life Sci* 2020;**1149**:122177.

24. Vainchtein LD, Rosing H, Schellens JH, Beijnen JH. A new, validated HPLC−MS/MS method for the simultaneous determination of the anti-cancer agent capecitabine and its metabolites: 5′-deoxy-5-fluorocytidine, 5′-deoxy-5-fluorouridine, 5-fluorouracil and 5-fluorodihydrouracil, in human plasma. *Biomed Chromatogr* 2010;**24**: 374−86.

25. Iusuf D, Ludwig M, Elbatsh A, van Esch A, van de Steeg E, Wagenaar E, et al. OATP1A/1B transporters affect irinotecan and SN-38 pharmacokinetics and carboxylesterase expression in knockout and humanized transgenic mice. *Mol Cancer Ther* 2014;**13**:492−503.

26. van de Steeg E, van der Kruijssen CM, Wagenaar E, Burggraaff JE, Mesman E, Kenworthy KE, et al. Methotrexate pharmacokinetics in transgenic mice with liver-specific expression of human organic anion-transporting polypeptide 1B1 (SLCO1B1). *Drug Metab Dispos* 2009; **37**:277−81.

27. Yang H, Wang H, Shivalila CS, Cheng AW, Shi L, Jaenisch R. One-step generation of mice carrying reporter and conditional alleles by CRISPR/Cas-mediated genome engineering. *Cell* 2013;**154**:1370−9.

28. Humerickhouse R, Lohrbach K, Li L, Bosron WF, Dolan ME. Characterization of CPT-11 hydrolysis by human liver carboxylesterase isoforms hCE-1 and hCE-2. *Cancer Res* 2000;**60**:1189−92.

29. Sanchez-Gurmaches J, Hung CM, Guertin DA. Emerging complexities in adipocyte origins and identity. *Trends Cell Biol* 2016; **26**:313−26.

30. Hegele RA. Plasma lipoproteins: genetic influences and clinical implications. *Nat Rev Genet* 2009;**10**:109−21.

31. Bahitham W, Watts R, Nelson R, Lian J, Lehner R. Liver-specific expression of carboxylesterase 1G/esterase-X reduces hepatic steatosis, counteracts dyslipidemia and improves insulin signaling. *Biochim Biophys Acta* 2016;**1861**:482−90.

32. Bie J, Zhao B, Marqueen KE, Wang J, Szomju B, Ghosh S. Macrophage-specific transgenic expression of cholesteryl ester hydrolase attenuates hepatic lipid accumulation and also improves glucose tolerance in *ob/ob* mice. *Am J Physiol Endocrinol Metab* 2012;**302**: E1283−91.

33. Xu Y, Zhu Y, Bawa FC, Hu S, Pan X, Yin L, et al. Hepatocyte-specific expression of human carboxylesterase 1 attenuates diet-induced steatohepatitis and hyperlipidemia in mice. *Hepatol Commun* 2020;**4**: 527−39.

34. Brestoff JR, Artis D. Immune regulation of metabolic homeostasis in health and disease. *Cell* 2015;**161**:146−60.

35. Gibbons GF, Wiggins D, Brown AM, Hebbachi AM. Synthesis and function of hepatic very-low-density lipoprotein. *Biochem Soc Trans* 2004;**32**:59−64.

36. Gilham D, Alam M, Gao W, Vance DE, Lehner R. Triacylglycerol hydrolase is localized to the endoplasmic reticulum by an unusual retrieval sequence where it participates in VLDL assembly without utilizing VLDL lipids as substrates. *Mol Biol Cell* 2005;**16**:984−96.